Eur. Phys. J. A **30**, 381–390 (2006)
DOI 10.1140/epja/i2006-10132-7

THE EUROPEAN PHYSICAL JOURNAL A

γ-ray spectroscopy of excited states in $^{61}_{30}Zn_{31}$

L-L. Andersson[1,a], D. Rudolph[1], J. Ekman[1,b], C. Fahlander[1], E.K. Johansson[1], R. du Rietz[1], C.J. Gross[2], P.A. Hausladen[2], D.C. Radford[2], and G. Hammond[3,c]

[1] Department of Physics, Lund University, S-221 00 Lund, Sweden
[2] Physics Division, Oak Ridge National Laboratory, Oak Ridge, TN 37830, USA
[3] School of Chemistry and Physics, Keele University, Keele, Staffordshire ST5 5BG, UK

Received: 22 June 2006 / Revised: 2 October 2006 /
Published online: 15 November 2006 –
Communicated by R. Krücken

Abstract. The $^{61}_{30}Zn_{31}$ isotope has been produced at the Oak Ridge National Laboratory in the fusion-evaporation reaction $^{40}Ca(^{24}Mg, 2pn)^{61}Zn$ at 104 MeV. The experimental set-up allowed γ-rays to be detected in the CLARION Ge detector array in coincidence with the detection of recoiling nuclei in the focal plane at the end of the recoil mass spectrometer. This provides a unique identification of γ-rays belonging to ^{61}Zn. The excited states have been explored by means of recoil-$\gamma\gamma$ coincidences, and the resulting decay scheme comprises almost 70 transitions. The data reveal numerous non-yrast states and suggest a revised spin and parity assignment for a previously observed superdeformed band. The resulting decay scheme is compared to predictions from different sets of large-scale shell model calculations.

PACS. 21.60.Cs Shell model – 23.20.En Angular distribution and correlation measurements – 23.20.Lv γ transitions and level energies – 27.40.+z $39 \leq A \leq 58$

1 Introduction

The $^{61}_{30}Zn_{31}$ nucleus lies just beyond the $N = Z = 28$ shell closure, with two protons and three neutrons occupying the subshells up to the next closure at $N = Z = 50$. The subshells placed in between the two shell closures are the negative-parity $2p_{3/2}$, $1f_{5/2}$ and $2p_{1/2}$ orbitals in the upper fp shell, and the positive-parity $\ell = 4$ $1g_{9/2}$ intruder orbital. Because of its high-j nature, excitations into the latter influence or even dominate the level sequences of $N \sim Z$, $A \simeq 60$ nuclei already at moderate excitation energies. Examples of this are ^{59,61}Cu and ^{61}Zn [1–3]. An additivity principle was derived in ref. [1], which relates the amount of quadrupole deformation to the number of particles in the $1g_{9/2}$ orbital and holes in the $1f_{7/2}$ orbital, providing a natural transition from spherical structures to superdeformed (SD) rotational sequences.

Theoretically, the inclusion of the $1g_{9/2}$ orbital in state-of-the-art shell-model calculations is difficult due to the center-of-mass problem, here caused by insufficient separation of center-of-mass and relative coordinates of the 61 nucleons (cf. p. 447 and p. 482ff in ref. [4]).

Another facet of $N \sim Z$, $A \simeq 60$ nuclei is the investigation of isospin symmetry by studying mirror nuclei, *i.e.* nuclei with the same mass number but with interchanged proton and neutron numbers. The mirror nucleus of $^{61}_{30}Zn_{31}$ is $^{61}_{31}Ga_{30}$, where the first few excited states recently have been established [5]. To obtain solid information on isospin-breaking effects from mirror nuclei, detailed spectroscopic knowledge of the less exotic partner —in this case ^{61}Zn— is necessary.

In the present paper we report on the investigation of excited states in ^{61}Zn. Previous data aimed to extend an existing [6,7] low-spin level scheme [2], to determine parity-changing $E1$ transitions [3], and to search for superdeformed rotational bands [8]. The most recent decay scheme of normally deformed structures in ^{61}Zn comprises some 25 γ-ray transitions reaching over 9 MeV excitation energy and a few spin and parity assignments [2], which were refined in ref. [3]. Our analysis provides a firm decay scheme with a considerable increase to almost 70 transitions ranging up to a spin $I^\pi = 31/2^-$ state at an excitation energy of $E_x = 10155$ keV. Interestingly, revised spin assignments of the low-lying levels based on ref. [3] and the current analysis affect the presumed, tentative spin assignments of the ^{61}Zn SD band [8].

[a] e-mail: lise-lotte.andersson@nuclear.lu.se
[b] *Present address:* Technology and Society, Malmö University, S-205 06 Malmö, Sweden.
[c] *Present address:* Department of Physics, University of York, Heslington, York, YO10 5DD, UK.

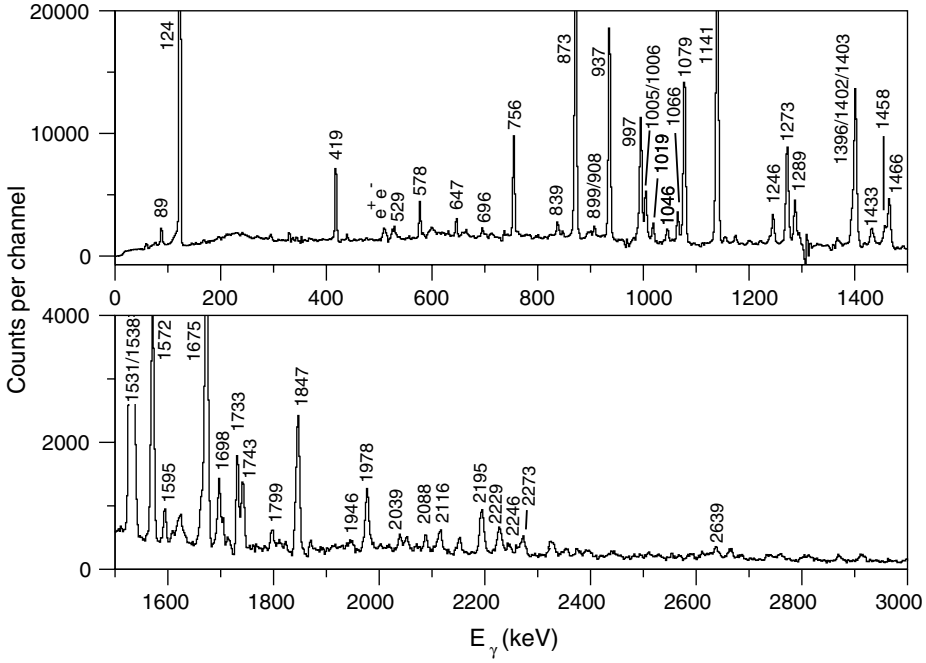

Fig. 1. Clean recoil-γ spectrum of ^{61}Zn. The most intense transitions are marked with energies in keV. The spectrum is binned to 2 keV/channel. See text for more details.

The experimentally observed energy levels in the ^{61}Zn nucleus are compared with shell model calculations using two different configuration spaces: i) the full fp space, neglecting excitations up to the $1g_{9/2}$ orbital, and ii) a closed ^{56}Ni core with the five valence nucleons moving in and between the $1f_{5/2}$, $2p_{3/2}$, $2p_{1/2}$, and $1g_{9/2}$ orbitals.

This paper reports on the experimental details including the set-up (sect. 2), the data analysis (sect. 3) and results (sect. 4). Section 5 deals with the shell model calculations involving both of the above-mentioned configuration spaces.

2 The experiment

The experiment was conducted at the Holifield Radioactive Ion Beam Facility (HRIBF) at Oak Ridge National Laboratory. In fusion-evaporation reactions of a 104 MeV ^{40}Ca beam, impinging on a 99.92% isotropically enriched ^{24}Mg target foil of thickness 0.3 mg/cm^2, ^{64}Ge compound nuclei are formed. The $^{61}_{30}$Zn$_{31}$ nuclei are then produced via the evaporation of two protons and one neutron.

The experimental set-up comprised the germanium detector array, CLARION [9], consisting of ten Ge clover detectors placed in a three ring configuration (90°, 132°, and 154°), and the Recoil Mass Spectrometer (RMS) using the split anode Ionisation Chamber (IC) at the focal plane [10]. The distance between the clover detectors and the target was 20.0 cm. In that configuration CLARION has an overall γ-ray detection efficiency of about 2.3% at 1.3 MeV γ-ray energy. At the end of the experiment CLARION was energy calibrated using the three standard γ-ray sources ^{152}Eu, ^{133}Ba, and ^{88}Y.

The combination of CLARION, RMS, and IC allows for correlations between γ-rays and residual nuclei providing a unique identification of γ-rays belonging to ^{61}Zn. The correlation was also used in the trigger conditions. An event was recorded only if one of two conditions was met: i) at least one Compton-suppressed γ-ray was detected in CLARION in coincidence with the detection of a recoil at the focal plane of the RMS or ii) two or more Compton-suppressed γ-rays were detected in the germanium detectors. More details about the set-up and data handling are described in ref. [5]. These include the Doppler and add-back corrections applied to the γ-ray data collected from the segmented 4-fold germanium clover detectors in CLARION.

The RMS separates the recoils in mass-to-charge ratio, A/Q, where Q denotes the charge state of the recoiling nuclei. For a given charge state masses are thus determined by their horizontal position at the focal plane of the spectrometer. These positions are measured by a position-sensitive grid, placed inside the IC. Information about the energy and the atomic number, Z, of the recoils is provided via the differential energy loss information from the split anode in the IC. This information is comprised in the R_{13} parameter, which relates the energy loss in the first and the third part of the IC anode via the ratio between the two. The R_{13} parameter is introduced and explained further in ref. [5].

3 Analysis

In total there are three isotopes of mass $A = 61$ observed in the present fusion-evaporation reaction; $^{61}_{29}$Cu$_{32}$, $^{61}_{30}$Zn$_{31}$,

Table 1. Excitation energies, γ-ray energies, relative intensities, and angular-distribution ratios for transitions in ^{61}Zn [6, 2, 3].

E_x (keV)	E_γ (keV)	I_γ (%)	R_{154-96}	I_i^π	I_f^π
88.8(2)	88.9(1)	3.0(1)	1.08(7)	$1/2^{-}$ [2]	$3/2^{-}$ [1]
123.9(2)	123.9(1)	100(3)	$\simeq 0.55$ [4]	$5/2^{-}$ [1]	$3/2^{-}$
419.2(2)	295.5(1)	0.6(1)	1.55(34)	$3/2^{-}$ [2]	$5/2^{-}$
	331.3(2)	1.2(1)	0.97(16)	$3/2^{-}$	$1/2^{-}$
	419.1(2)	8.9(3)	1.11(6)	$3/2^{-}$	$3/2^{-}$
756.4(3)	339.0(2)	0.9(1)	—	$5/2^{-}$ [2]	$3/2^{-}$
	631.7(3)	1.1(1)	0.72(16)	$5/2^{-}$	$5/2^{-}$
	666.6(3)	1.8(1)	—	$5/2^{-}$	$1/2^{-}$
	755.7(4)	18(1)	0.60(3)	$5/2^{-}$	$3/2^{-}$
997.7(4)	241.4(1)	0.5(1)	—	$7/2^{-}$ [1]	$5/2^{-}$
	578.2(3)	4.4(2)	1.40(9)	$7/2^{-}$	$3/2^{-}$
	872.7(4)	73(2)	0.64(3)	$7/2^{-}$	$5/2^{-}$
	996.7(5)	27(6)	1.48(7) [3]	$7/2^{-}$	$3/2^{-}$
1266(1)	1141(1)	83(3)	1.62(7)	$9/2^{-}$ [1]	$5/2^{-}$
1403(1)	647.1(3)	3.4(1)	0.66(6)	$7/2^{-}$ [2]	$5/2^{-}$
	984.3(5)	3.5(5)	—	$7/2^{-}$	$3/2^{-}$
	1278(1)	2.0(1)	1.01(12)	$7/2^{-}$	$5/2^{-}$
	1403(1)	5.3(31)	0.84(4) [3]	$7/2^{-}$	$3/2^{-}$
2003(1)	737.6(4)	1.0(1)	—	$9/2^{-}$ [2]	$9/2^{-}$
	1006(1)	8.5(10)	0.37(2) [3]	$9/2^{-}$	$7/2^{-}$
	1246(1)	8.1(3)	1.40(8)	$9/2^{-}$	$5/2^{-}$
2270(1)	1005(1)	10(1)	0.37(2) [3]	$11/2^{-}$ [1]	$9/2^{-}$
	1273(1)	27(1)	1.77(8)	$11/2^{-}$	$7/2^{-}$
2400(1)	997.0(5)	5(3)	1.48(7) [3]	$9/2^{+1}$	$7/2^{-}$
	1403(1)	41(5)	0.84(4) [3]	$9/2^{+}$	$7/2^{-}$
	2273(1)	2.3(1)	1.17(16)	$9/2^{+}$	$5/2^{-}$
2699(2)	696.2(3)	1.7(1)	0.70(13)	$11/2^{-}$	$9/2^{-}$
	1433(1)	6.7(2)	1.01(6)	$11/2^{-}$	$9/2^{-}$
2799(2)	529.4(3)	0.8(1)	—	$13/2^{-}$ [1]	$11/2^{-}$
	1531(1)	46(3)	1.70(7) [3]	$13/2^{-}$	$9/2^{-}$
3244(2)	1978(1)	7.7(3)	0.78(6)	$11/2^{+1}$	$9/2^{-}$
3336(1)	936.7(5)	39(2)	1.70(7)	$13/2^{+1}$	$9/2^{+}$
	1066(1)	6.9(2)	0.98(6)	$13/2^{+}$	$11/2^{-}$
3461(2)	1458(1)	6.6(3)	1.51(9)	$13/2^{-}$	$9/2^{-}$
	2195(1)	5.5(3)	1.60(11)	$13/2^{-}$	$9/2^{-}$
3495(3)	2229(1)	3.4(1)	1.40(12)	—	$9/2^{-}$
3844(2)	1046(1)	4.2(1)	—	$15/2^{-}$ [1]	$13/2^{-}$
	1572(1)	16(1)	1.62(8)	$15/2^{-}$	$11/2^{-}$
4264(2)	1019(1)	3.6(1)	1.73(13)	$15/2^{+1}$	$11/2^{+}$
	1466(1)	19(1)	0.73(4)	$15/2^{+}$	$13/2^{-}$
4309(3)	2039(1)	1.9(1)	0.87(14)	13/2	$11/2^{-}$
4415(2)	1079(1)	35(1)	1.76(7)	$17/2^{+1}$	$13/2^{+}$
4644(2)	1847(1)	11(1)	1.66(9)	$17/2^{-}$ [1]	$13/2^{-}$
4915(3)	2116(1)	3.4(1)	0.81(9)	—	$13/2^{-}$
5195(3)	1733(1)	3.5(11)	1.49(10) [3]	$17/2^{-}$	$13/2^{-}$
5254(2)	839.2(4)	3.1(1)	1.18(10)	—	$17/2^{+}$
	990.9(5)	1.4(3)	1.32(13) [3]	—	$15/2^{+}$
5468(3)	1624(1)	3.6(1)	—	—	$15/2^{-}$
5543(2)	898.9(4)	2.1(7)	—	$19/2^{-}$ [1]	$17/2^{-}$
	1698(1)	5.8(3)	1.57(10)	$19/2^{-}$	$15/2^{-}$
5552(2)	908.3(5)	2.6(1)	0.62(10)	$19/2^{+1}$	$17/2^{-}$
	1289(1)	11(1)	1.67(9)	$19/2^{+}$	$15/2^{+}$
6090(2)	1675(3)	22(2)	1.69(8) [3]	$21/2^{+1}$	$17/2^{+}$
6212(3)	1799(1)	2.3(6)	—	—	$17/2^{+}$
	1946(1)	1.4(1)	—	—	$15/2^{+}$

Table 1. Continued.

E_x (keV)	E_γ (keV)	I_γ (%)	R_{154-96}	I_i^π	I_f^π
7284(2)	1733(1)	1.2(3)	1.49(10) [3]	$21/2^{-}$	$19/2^{+}$
	2088(1)	1.7(1)	1.32(17)	$21/2^{-}$	$17/2^{-}$
	2639(1)	2.1(9)	—	$21/2^{-}$	$17/2^{-}$
7295(3)	1743(1)	5.4(3)	1.47(10)	$23/2^{+1}$	$19/2^{+}$
7486(3)	1396(1)	9.9(4)	1.93(10)	$25/2^{+1}$	$21/2^{+}$
7629(2)	344.8(2)	0.3(1)	1.20(24)	$23/2^{-1}$	$21/2^{-}$
	1538(1)	7.5(7)	0.60(6)	$23/2^{-}$	$21/2^{+}$
8336(3)	2246(1)	0.9(1)	—	—	$21/2^{+}$
8496(4)	1201(1)	2.2(1)	—	—	$23/2^{+}$
8777(3)	440.6(2)	0.5(1)	0.71(18)	—	—
8879(3)	1595(1)	1.9(1)	1.79(21)	$25/2^{-}$	$21/2^{-}$
9161(3)	1532(1)	6.3(7)	1.70(7) [3]	$27/2^{-1}$	$23/2^{-}$
	1675(4)	4.0(20)	1.69(8) [3]	$27/2^{-}$	$25/2^{+}$
10155(3)	994.1(5)	3.4(6)	1.48(7) [3]	$31/2^{-1}$	$27/2^{-}$

[1] Spin and parity supported or adopted from ref. [3].
[2] Spin and parity supported or adopted from ref. [6].
[3] Doublet structure.
[4] Ratio corrected using the estimated lifetime of the state.

and $^{61}_{31}Ga_{30}$. Since the recoils have different proton numbers the energy loss signals will peak at slightly different values of R_{13}. Hence, it is possible to increment γ-ray spectra containing predominately recoils of only one species. This is done by restricting the values of R_{13} around the known peak positions for ^{61}Cu, ^{61}Zn, and ^{61}Ga, respectively. Performing a careful fractional subtraction makes it possible to obtain clean γ-ray spectra for the three $A = 61$ recoils. The resulting clean ^{61}Zn spectrum is shown in fig. 1. Only at 1310 keV, an effect of the fractional subtraction can be seen. The fluctuations are a result of the subtraction of the most intense peak in ^{61}Cu, which is the strongest of the $A = 61$ reaction channels.

From the clean ^{61}Zn spectrum transitions have been identified, their energies have been determined, and relative intensities have been obtained. The results are listed in table 1. Intensities, I_γ, in the table are both efficiency corrected and corrected for the mean angular position of all detectors. At a mean position of $\bar{\theta} \approx 55^\circ$ the relative intensities of $\Delta I = 0$, 1, and 2 transitions are equal [11]. In CLARION the mean position is at $\bar{\theta} = 65^\circ$ and correction factors to account for the non-equal detection have to be determined. By evaluating angular distributions calculated with alignment coefficients, σ, typical for fusion-evaporation reactions, correction factors of 1.09(2) and 0.95(2) for $\Delta I = 0$, 2 and $\Delta I = 1$ transitions, respectively, have been derived. These are included in the values in table 1.

The data from this experiment was incorporated in so-called recoil-$\gamma\gamma$ matrices, which were used to establish coincidences between γ-ray transitions. As the name implies, the $\gamma\gamma$-matrices are gated by recoils, *i.e.*, they contain only γ-rays observed in coincidence with the detection of an $A = 61$ recoil in the focal plane. Two matrices were constructed; one with R_{13}-values compatible with ^{61}Zn and the other compatible with ^{61}Cu. This restriction aimed to minimise the amount of contaminants. The

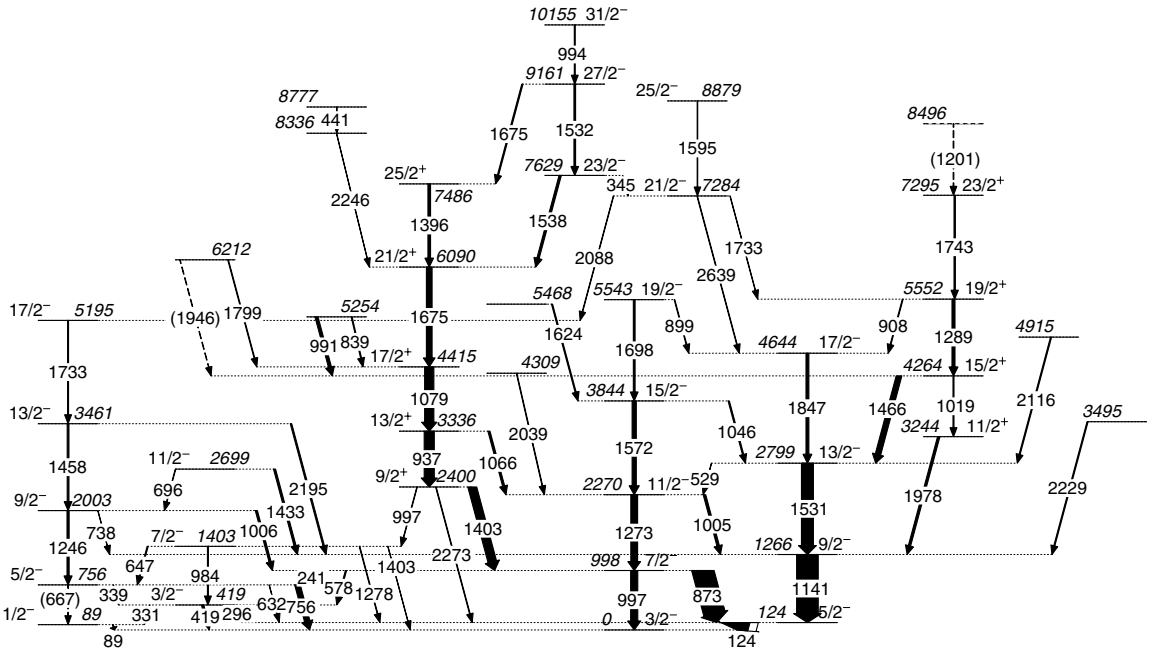

Fig. 2. The decay scheme of ^{61}Zn from the present work. Energy labels are in keV and the intensities of the transitions are here indicated by the relative thicknesses of the arrows. Tentative levels and transitions are dashed.

presence of ^{61}Cu (^{61}Zn) recoils in the ^{61}Zn (^{61}Cu) gated matrix is, however, unavoidable due to the partially overlapping R_{13}-values of the two species. Coincidence spectra obtained by identically selecting a specific transition in the two matrices, can be subtracted from each other in a similar manner as previously described for the spectrum in fig. 1. This results in an "isotopic" $\gamma\gamma$ analysis of the ^{61}Zn transitions.

The careful coincidence analysis using the recoil-$\gamma\gamma$ matrices described above has been carried out for the ^{61}Zn nucleus. Figures 3, 4, and 5 show examples of coincidence spectra, both for intense and weak transitions. As can be seen from the figures, coinciding γ-ray transitions are easily determined from these very clean spectra. The coincidence information has been used to build the comprehensive decay scheme of ^{61}Zn, illustrated in fig. 2. A few transitions, which have not been possible to place into the decay scheme due to lack of statistics, remain unmarked in fig. 1.

Intensity ratios of γ-rays observed in different detector rings in the set-up [5] are also included in table 1. In the current analysis this ratio, R_{154-96}, is determined for the detectors placed at 84°, 96°, with respect to the beam axis, and those placed at 148°, 160°. Due to the dependence of the angular distribution on detector position the latter detectors may be treated as having an average detector position of 154°. The former, due to the symmetry at 90°, must be kept at either of the two positions, since they are placed symmetrically around 90°. Hence, R_{154-96} gives the ratio of yields, Y, between two of the detector rings in CLARION. Ratios for known stretched $\Delta I = 2$ reference transitions amount to $R_{154-96} = Y(154°)/Y(96°) \sim 1.6$–$1.7$, while stretched dipole transitions have $R_{154-96} \sim 0.7$–0.8. In order to assign both spin and parity to the levels the previously published assignments from ref. [3], investigated by means of angular correlations (DCO-ratios) and linear polarisations, and ref. [6] have been included. The previous assignments are confirmed by the angular distributions found in the current experiment. Additional levels have been assigned spin and parity based on angular distributions from the current analysis and yrast arguments.

Two things from table 1 are worth extra attention. First note the 124 keV level, which is fed with a total intensity of 160(4) units, but with a total decay of only 100(3) units. The large discrepancy can be explained by the combined effect of internal conversion of the 124 keV γ-ray and a relatively long lifetime of the 124 keV state. In fact, both these effects are coupled to each other via the R_{154-96} value of this transition. The experimentally obtained value is $R_{154-96} = 0.91(4)$. This value indicates either an almost pure $\Delta I = 1$ dipole transition or an almost pure $\Delta I = 1$ quadrupole transition. The conversion coefficients in these two extreme cases are $\alpha = 0.04$ and $\alpha = 0.32$, respectively. Thus, even in the case of a pure quadrupole transition internal conversion can only account for a fraction of the missing yield. The remaining portion of about 30(6) units is attributed to a relatively long lifetime of the 124 keV state, which is estimated in the following.

Arrays of Ge detectors such as CLARION reach their full efficiency only if the γ-rays are emitted at the target position. If the recoiling nuclei γ decay at a position, d, behind the target, only a fraction, $\Omega(d)$, of the maximal solid angle, Ω_0, is accessible. Clearly, $\Omega(d)$ depends on the detector position, *i.e.* $\Omega(d) = \Omega(d, \theta)$. With a proper calibration isomeric states can be measured via this "shadowing" of the germanium detectors [12]. In this analysis, however, only an estimation of the lifetime can be ob-

tained as there are no calibration points. The function $\Omega(d,\theta)$ has been simulated and then replaced by the approximative assumption

$$\Omega(d,\theta) = \begin{cases} \Omega_0, & d \le D_0(\theta), \\ 0, & d > D_0(\theta), \end{cases}$$

with $D_0(96°) = 8\,\mathrm{cm}$, $D_0(132°) = 16\,\mathrm{cm}$, $D_0(154°) = 22\,\mathrm{cm}$ and $D_0(\bar{\theta}) = 13\,\mathrm{cm}$. Using the latter, the missing yield, and knowing the average velocity $v/c = 4.26(1)\%$ for the recoils, the lifetime, τ, can be estimated. In case of a pure dipole (quadrupole) transition one obtains $\tau \approx 10\,\mathrm{ns}$ ($\tau \approx 6\,\mathrm{ns}$). The experimentally obtained intensities of the 124 keV line in the different detector rings hence lack yield due to recoils in the long-lived state moving away from the target position before decaying. Consequently, the experimentally obtained R_{154-96} needs to be corrected. The correction factors obviously depend on τ and, hence, on the multipolarity of the transition. In case of a pure dipole transition the correction factors are 1.2 (154°) and 2.2 (96°), and in case of a quadrupole character they are 1.1 and 1.6, respectively. This results in a corrected R_{154-96} value of about 0.5 (dipole) and 0.6 (quadrupole). Using an average of these values provides some kind of self-consistent estimate for the involved quantities: $R_{154-96} \approx 0.55$ and $\tau \approx 8\,\mathrm{ns}$ gives a $\delta(E2/M1) \approx 1$ mixing of this transition.

The second remark from table 1 concerns the "double doublet" structure of the yrare and yrast 1403 keV and the yrare and yrast 997 keV transitions, which in parallel depopulate the $9/2^+$ level at 2400 keV. The 1403 keV energy level and the transition into the ground state are previously known [6]. First of all, gating on the 997 keV and the 873 keV transitions in the current data set results in a non-equal ratio between the yields of the 1273 keV and the 1403 keV γ-ray transitions, which feed the 998 keV level. In fact, the gate reveals a larger amount of the 1403 keV transition in the 997 keV gate than in the 873 keV gate. This provides first evidence for the two yrare transitions in the "double doublet" structure. The determination is, however, complicated by the energetically close 1396 and 994 keV transitions.

To obtain reasonable values of the relative intensities of the four transitions it is necessary to make indirect measurements. From the spectrum in coincidence with the 1273 keV transition the branching ratio between the yrast 997 keV and the 873 keV transitions could be obtained. The 873 keV γ-ray transition is well established, but difficulties arise from the 994 keV $31/2^- \rightarrow 27/2^-$ transition, which is close in energy to the 997 keV transitions and impossible to separate completely. In a similar way, the branching ratio between the 1273 and the yrast 1403 keV transitions might be obtained from the spectrum in coincidence with the 873 keV transition. Difficulties, however, arise from the energetically close-lying 1396 keV $25/2^+ \rightarrow 21/2^+$ transitions, which can affect the ratio of yields.

While the intensities of the two yrast transitions can be determined reasonably well with the described procedure, it turns out to be basically impossible to obtain meaningful numbers for the yrare transitions from the current data set. However, using information from an independent, early data set taken with the GAMMASPHERE array, the estimates included in table 1 can be derived for the yrare transitions [13].

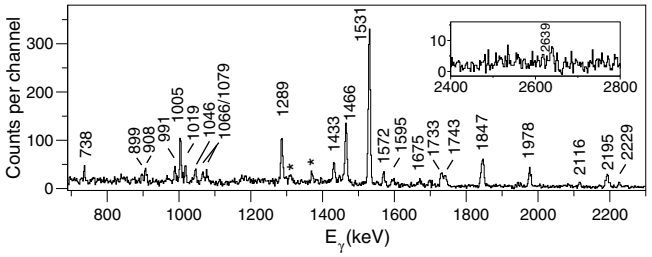

Fig. 3. Recoil-$\gamma\gamma$ spectrum in coincidence with $A = 61$, $Z = 30$ identified in the RMS, and the intense 1141 keV $9/2^- \rightarrow 5/2^-$ yrast transition. All peaks marked with an energy label are placed into the decay scheme of fig. 2, while stars denote minor contaminations from ^{61}Cu. The spectrum is binned to 2 keV/channel.

4 Results

In fig. 3 transitions in coincidence with the intense 1141 keV $9/2^- \rightarrow 5/2^-$ γ-ray are illustrated. The previously known [3] negative-parity yrast sequence 1847, 1531, 1141 keV can easily be seen in the figure via the first two γ-rays. Spin and parity of this sequence are well determined (see ref. [3] and table 1). In fig. 3 the 1743, 1289, and 1019 keV transitions between positive-parity yrast states are illustrated. The spin and parity assignments of the involved energy levels differ between ref. [2] and ref. [3], while the present analysis supports the 11/2 assignment of the 3244 keV level by the $\Delta I = 2$ 1019 keV and the $\Delta I = 1$ 1466 and 1978 keV transitions. The two sequences mentioned above are connected via three transitions at 1978, 1466, and 908 keV, respectively. Peaks at these energies are also present in fig. 3. The high-lying levels at 8879 and 7284 keV from fig. 2 are established indirectly in the coincidence spectrum of fig. 3, via the 1595 keV transition between them and the 1733 keV transition connecting them to the $19/2^+$ level. Spin and parity of the level at 7284 keV are determined via its connection both to the positive-parity band to the right and the negative-parity band to the far left in fig. 2. The 2088 keV transition can be used as guidance due to its likely $\Delta I = 2$ character. The 1733 keV transition, however, is unreliable due to its doublet structure. The 2639 keV $21/2^- \rightarrow 17/2^-$ transition, visible in fig. 2, is not very intense but can be distinguished in a close-up view of the spectrum.

Figure 4 illustrates the coincidences with the 1675 keV, $21/2^+ \rightarrow 17/2^+$, and $27/2^- \rightarrow 25/2^+$, doublet structure. The two transitions are found to be self-coincident. The lower 1675 keV transition is placed in the clearly visible 937, 1079, 1675, and 1396 keV sequence, present in the figure, while the upper 1675 keV transition is feeding it.

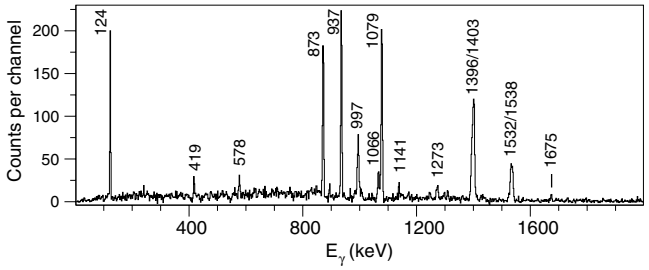

Fig. 4. Same as fig. 3 but in coincidence with the 1675 keV $21/2^+ \rightarrow 17/2^+$ and the 1675 keV $27/2^- \rightarrow 25/2^+$ yrast transitions.

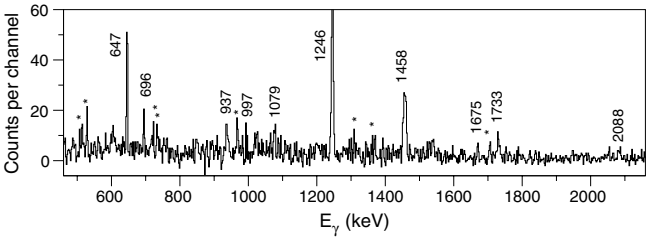

Fig. 5. Same as fig. 3 but in coincidence with the 756 keV $5/2^- \rightarrow 3/2^-$ ground-state transition. The low intensity of this transition in combination with the energetically close 762 keV transition in ^{61}Cu makes the contaminating transitions much more intense than in the previous figures.

The positive parity of the lower 1675 keV transition's band has already been established via the clear $E1$ properties of both the 1403 keV and the 1066 keV transitions [3]. In the same paper the 1538 keV transition has been established, causing the connected energy level at 7629 keV to have spin and parity $23/2^-$. Combining this with the $E2$ character of the 1396 keV transition determines the upper 1675 keV transition to decay from $27/2^-$ down to a $25/2^+$ level. The properties of the 1532 keV transition are not as reliable due to the close placement of the 1531 keV $13/2^- \rightarrow 9/2^-$ doublet transition.

Figure 5 illustrates the γ-rays in coincidence with the 756 keV $5/2^- \rightarrow 3/2^-$ ground-state transition. The spectrum contains more contaminating transitions from ^{61}Cu than previous figures. This is a result of the combined effect of gating on a relatively weak transition in ^{61}Zn and having an energetically close (762 keV) transition in ^{61}Cu. In spite of the contamination of ^{61}Cu in the gate the ^{61}Zn information is clear. Two transitions decay into the 756 keV energy level, the 1246 and 647 keV transitions, both clearly visible in this spectrum. The subsequent 1458, 1733 and 2088 keV transitions are all three also illustrated in the figure. Even the positive-parity yrast sequence of 1675, 1079, 937 keV transitions are indicated in this spectrum, all decaying into the 756 keV energy level via the earlier mentioned, difficult 997 keV γ-ray transition. This weak transition is indirectly established by the presence of these transitions in the coincidence spectrum.

5 Shell model interpretation

The experimental results can be compared with predictions obtained from large-scale shell model calculations using the code ANTOINE [14,15]. In the present paper two calculations have been carried out.

The first calculation involves the $1f_{7/2}$ orbit below the $N = Z = 28$ shell closures and the $2p_{3/2}$, $1f_{5/2}$, and $2p_{1/2}$ orbits above —here referred to as the fp calculation. No positive-parity states will be obtained for ^{61}Zn in this calculation as the configuration space includes only odd-ℓ orbitals. The interaction, GXPF1 [16,17], is adjusted to nuclei beyond the $N = Z = 28$ shell closure. In the current calculation no Coulomb interaction was included and the configuration space was truncated to allow up to three particle excitations from the $1f_{7/2}$ shell into the upper fp shell.

The second calculation uses a ^{56}Ni core and allows only excitations outside the core, *i.e.*, neglecting the $1f_{7/2}$ orbit. On the other hand, it includes the $1g_{9/2}$ orbit, and it is referred to as the $f_{5/2}pg_{9/2}$ calculation in the following. This interaction is derived from the Bonn-C nucleon-nucleon interaction and adjusted for the $Z > 28$, $N < 50$ region [18] in a similar fashion as it was done for GXPF1 within the fp shell [16,17].

In fig. 6 the experimental level energies are compared with the predicted energies from the two calculations. In the middle and on the right-hand side of the figure the negative- and positive-parity yrast states are shown. On the left-hand side the negative-parity yrare states are illustrated. Third states of a given spin-parity combination are not included in the figure because there are essentially no experimentally well-defined states.

The energy levels from the fp calculation agree very well with the experimental states up to spin and parity $19/2^-$. However, at higher spins the levels clearly mismatch. These difficulties are expected, since the influence of the $1g_{9/2}$ orbital becomes more and more important when forming high-spin states in ^{61}Zn [1] due to its high-j nature.

The opposite situation is true for the $f_{5/2}pg_{9/2}$ calculation. The lack of the $1f_{7/2}$ orbital in the calculation may explain difficulties to reproduce low-spin states but a significantly better agreement than for the fp calculation is found at high spins. Figure 6 illustrates this for the negative-parity yrast levels where the predictions improve above spin 19/2. The $f_{5/2}pg_{9/2}$ calculation also reproduces positive-parity yrast states well.

The Mean Level Deviation (MLD) measures how well the calculated energy levels match the experimental states. Normalising to the ground states, the MLD is here calculated as

$$\mathrm{MLD} = \sqrt{\frac{\sum_i (E_{x_i} - E_{th_i})^2}{n}}\,, \qquad (1)$$

where E_{x_i} and E_{th_i} are the experimentally observed and predicted energies, respectively, and n corresponds to the number of levels included in the MLD calculation.

For the fp calculation the MLD is 1561 keV if all yrare and yrast levels are included. The magnitude of this value

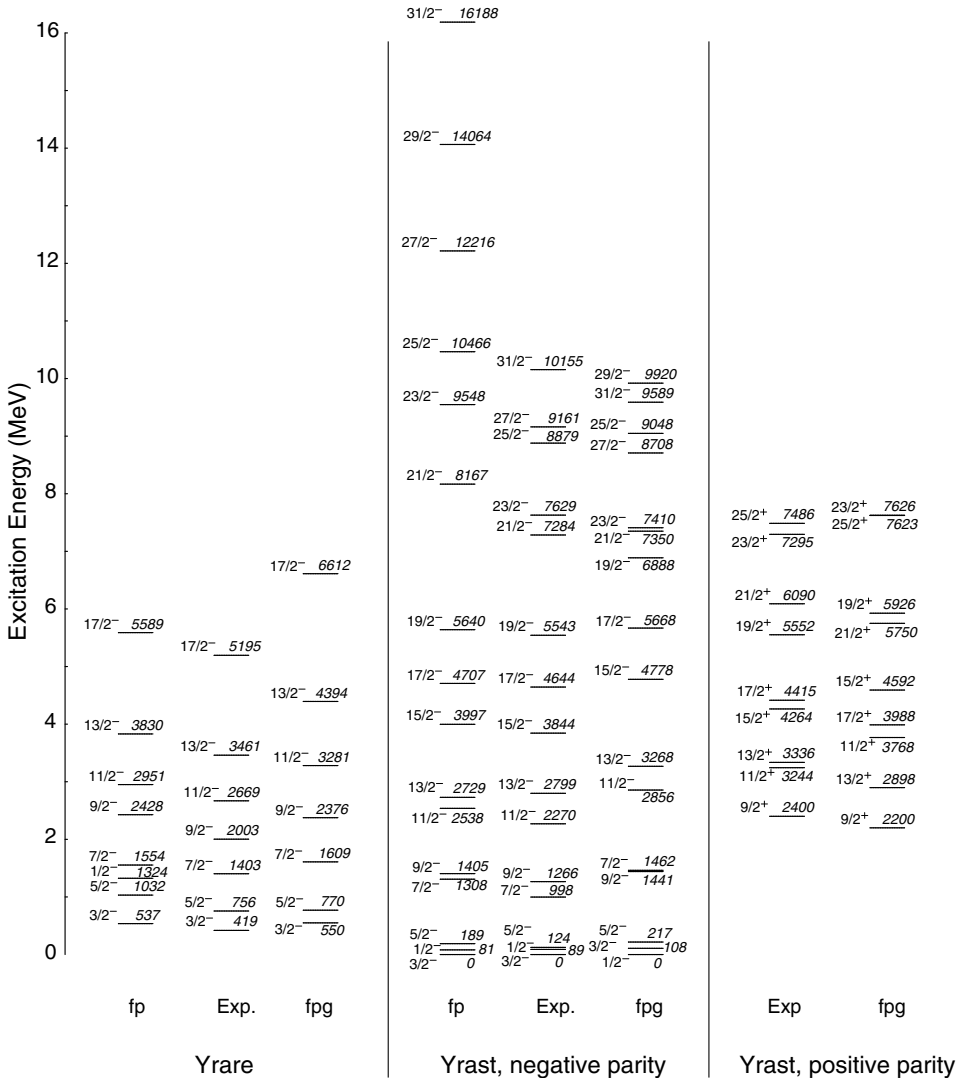

Fig. 6. Comparison between the experimental and calculated levels from the fp and fpg shell model calculation. The middle section illustrates the negative-parity yrast levels. On the right-hand side are the positive-parity yrast, and on the left-hand side are the negative-parity yrare states. See text for details.

suggests a poor agreement between experiment and theory. If only levels up to spin 19/2 are included the corresponding number drops dramatically to 228 keV, suggesting good agreement. Calculating MLD for only yrast levels up to spin 19/2 results in an even lower value of 153 keV. MLD values for the $f_{5/2}pg_{9/2}$ calculation are 569 keV if all yrast and yrare levels are included and including only yrast levels an MLD of 523 keV is obtained. A calculation of only levels above 19/2 results in a MLD of 307 keV.

Figure 6 illustrates in a simple way that neither of the two calculations used in this analysis are adequate to fully describe ^{61}Zn. Both holes in the $1f_{7/2}$ orbit and particles in the $1g_{9/2}$ orbit seem necessary in order for the calculation to truly reproduce the experimentally obtained nuclear energy levels. Calculations involving both orbitals are, however, impossible to carry out at present, due to the center-of-mass difficulties [4] mentioned earlier.

In the current analysis a more thorough investigation of the wave functions calculated by ANTOINE has been carried out. This analysis involves the electromagnetic decay properties of the nuclear states and is done using the free g-factors and effective charges of $0.5e$ ($1.5e$) for neutrons (protons). Applying the g-factors and the charges via the $B(M1)$ and $B(E2)$ values obtained for each transition enables a study of branching ratios b. Experimentally obtained relative strengths are compared to the calculated branching ratios and the results are illustrated in table 2. Here, all possible transitions, $\Delta I = 0, 1, 2$, have been investigated, including those transitions, which are predicted to be energetically allowed, but which have not been experimentally observed.

Generally, the results from the analysis of the electromagnetic decay properties show good agreement with the experimental data in the fp calculation both for the yrast and the yrare states below $I^\pi = 19/2^-$. An example

Table 2. Comparison between experimental and predicted branching ratios, b, of the γ-rays in ^{61}Zn. Two shell model calculations have been compared in this analysis. b_{fp} denotes the branching ratios from the fp calculation and b_{fpg} from the $f_{5/2}pg_{9/2}$ calculation. Transitions written in italic style are experimentally not observed (n.o.). See text for more details.

E_x (keV)	E_γ (keV)	I_i^π	I_f^π	b_{exp}	b_{fp}	b_{fpg}
88.8	89	$1/2_1^-$	$3/2_1^-$	1.0	1.0	1.0
123.9	*35*	$5/2_1^-$	$1/2_1^-$	n.o.	0.00	0.03
	124		$3/2_1^-$	1.0	1.0	0.97
419.2	296	$3/2_2^-$	$5/2_1^-$	0.06(1)	0.02	0.09
	331		$1/2_1^-$	0.11(1)	0.04	0.43
	419		$3/2_1^-$	0.83(2)	0.94	0.48
756.4	339	$5/2_2^-$	$3/2_2^-$	0.04(1)	0.05	0.01
	632		$5/2_1^-$	0.05(1)	0.07	0.04
	667		$1/2_1^-$	0.08(1)	0.00	0.00
	756		$3/2_1^-$	0.83(2)	0.88	0.95
997.7	241	$7/2_1^-$	$5/2_2^-$	n.o.	0.00	0.00
	578		$3/2_2^-$	0.04(1)	0.11	0.06
	873		$5/2_1^-$	0.70(5)	0.88	0.02
	997		$3/2_1^-$	0.26(5)	0.01	0.91
1266	*268*	$9/2_1^-$	$7/2_1^-$	n.o.	0.03	0.00
	510		$5/2_2^-$	n.o.	0.00	0.00
	1141		$5/2_1^-$	1.0	0.97	1.0
1403	*137*	$7/2_2^-$	$9/2_1^-$	n.o.	0.00	0.00
	405		$7/2_1^-$	n.o.	0.00	0.00
	647		$5/2_2^-$	0.24(5)	0.32	0.10
	984		$3/2_2^-$	0.25(7)	0.00	0.45
	1278		$5/2_1^-$	0.14(3)	0.05	0.14
	1403		$3/2_1^-$	0.37(19)	0.63	0.30
2003	*600*	$9/2_2^-$	$7/2_2^-$	n.o.	0.09	0.01
	738		$9/2_1^-$	0.06(1)	0.33	0.02
	1006		$7/2_1^-$	0.48(4)	0.27	0.02
	1246		$5/2_2^-$	0.46(4)	0.28	0.95
	1879		$5/2_1^-$	n.o.	0.02	0.00
2270	*267*	$11/2_1^-$	$9/2_2^-$	n.o.	0.00	0.00
	867		$7/2_2^-$	n.o.	0.00	0.03
	1005		$9/2_1^-$	0.27(3)	0.25	0.01
	1273		$7/2_1^-$	0.73(3)	0.75	0.96
2400	997	$9/2_1^+$	$7/2_2^-$	0.10(6)	—	—
	1403		$7/2_1^-$	0.85(15)	—	—
	2273		$5/2_1^-$	0.05(1)	—	—
2699	*276*	$11/2_2^-$	$7/2_3^-$	n.o.	0.00	—
	429		$11/2_1^-$	n.o.	0.00	0.00
	696		$9/2_2^-$	0.20(1)	0.19	0.01
	1433		$9/2_1^-$	0.80(1)	0.44	0.00
	1296		$7/2_2^-$	n.o.	0.33	0.68
	1701		$7/2_1^-$	n.o.	0.04	0.30
2799	*100*	$13/2_1^-$	$11/2_2^-$	n.o.	0.00	0.00
	529		$11/2_1^-$	0.02(1)	0.00	0.00
	796		$9/2_2^-$	n.o.	0.00	0.00
	1531		$9/2_1^-$	0.98(1)	1.00	1.00
3244	1978	$11/2_1^+$	$9/2_1^-$	1.0	—	—
3336	937	$13/2_1^+$	$9/2_1^+$	0.85(7)	—	1.00
	1066		$11/2_1^-$	0.15(1)	—	—
3461	*662*	$13/2_2^-$	$13/2_1^-$	n.o.	0.03	0.01
	762		$11/2_2^-$	n.o.	0.04	0.01
	820		$9/2_3^-$	n.o.	0.00	—
	1191		$11/2_1^-$	n.o.	0.00	0.00
	1458		$9/2_2^-$	0.55(2)	0.24	0.99
	2195		$9/2_1^-$	0.45(2)	0.69	0.00
3495(3)	*34*	$11/2_3^-$	$13/2_2^-$	n.o.	0.00	0.00
	696		$13/2_1^-$	n.o.	0.09	0.32
	796		$11/2_2^-$	n.o.	0.02	0.00
	854		$9/2_3^-$	n.o.	0.00	—
	1079		$7/2_3^-$	n.o.	0.00	—
	1225		$11/2_1^-$	n.o.	0.07	0.00
	1492		$9/2_2^-$	n.o.	0.11	—
	2092		$7/2_2^-$	n.o.	0.02	—
	2229(1)		$9/2_1^-$	1.0	0.59	—
	2497		$7/2_1^-$	n.o.	0.08	—
3844	*349*	$15/2_1^-$	$11/2_3^-$	n.o.	0.00	—
	383		$13/2_2^-$	n.o.	0.00	0.00
	1046		$13/2_1^-$	0.21(1)	0.16	0.00
	1145		$11/2_2^-$	n.o.	0.01	0.00
	1572		$11/2_1^-$	0.79(1)	0.83	1.0
4264	*928*	$15/2_1^+$	$13/2_1^+$	n.o.	—	0.00
	1019		$11/2_1^+$	0.16(1)	—	1.0
	1466		$13/2_1^-$	0.84(6)	—	—
4309(3)	*465*	$13/2_3^-$	$15/2_1^-$	n.o.	0.04	—
	814		$11/2_3^-$	n.o.	0.10	—
	848		$13/2_2^-$	n.o.	0.01	—
	1510		$13/2_1^-$	n.o.	0.08	—
	1610		$11/2_2^-$	n.o.	0.01	—
	1668		$9/2_3^-$	n.o.	0.20	—
	2039(1)		$11/2_1^-$	1.0	0.36	—
	2306		$9/2_2^-$	n.o.	0.17	—
	3043		$9/2_1^-$	n.o.	0.04	—
4415	*151*	$17/2_1^+$	$15/2_1^+$	n.o.	—	0.00
	1079		$13/2_1^+$	1.0	—	1.0
4644	*335*	$17/2_1^-$	$13/2_3^-$	n.o.	0.00	0.00
	800		$15/2_1^-$	n.o.	0.01	0.00
	1183		$13/2_2^-$	n.o.	0.03	0.00
	1847		$13/2_1^-$	1.0	0.95	1.0
4915(3)	*271*	$15/2_3^-$	$17/2_1^-$	n.o.	0.00	0.03
	606		$13/2_3^-$	n.o.	0.16	0.05
	1071		$15/2_1^-$	n.o.	0.04	0.00
	1420		$11/2_3^-$	n.o.	0.03	0.85
	1454		$13/2_2^-$	n.o.	0.01	0.00
	2116(1)		$13/2_1^-$	1.0	0.69	0.00
	2216		$11/2_2^-$	n.o.	0.04	0.01
	2645		$11/2_1^-$	n.o.	0.02	0.07
5195	*208*	$17/2_2^-$	$15/2_3^-$	n.o.	0.01	0.00
	551		$17/2_1^-$	n.o.	0.02	0.27
	886		$13/2_3^-$	n.o.	0.01	0.03
	1351		$15/2_1^-$	n.o.	0.08	0.01
	1733		$13/2_2^-$	1.0	0.64	0.06
	2396		$13/2_1^-$	n.o.	0.25	0.63

Table 2. Continued.

E_x (keV)	E_γ (keV)	I_i^π	I_f^π	b_{exp}	b_{fp}	b_{fpg}
5543	*75*	$19/2_1^-$	$17/2_3^-$	n.o.	0.00	0.00
	348		$17/2_2^-$	n.o.	0.00	0.00
	628		$15/2_3^-$	n.o.	0.00	0.00
	899		$17/2_1^-$	0.27(7)	0.09	0.00
	1698		$15/2_1^-$	0.73(7)	0.91	1.0
5552	908	$19/2_1^+$	$17/2_1^-$	0.19(2)	—	—
	1289		$15/2_1^+$	0.81(9)	—	1.0
6090	*538*	$21/2_1^+$	$19/2_1^+$	n.o.	—	0.00
	704		$17/2_2^+$	n.o.	—	0.00
	1675		$17/2_1^+$	1.0	—	1.0
7284	*629*	$21/2_1^-$	$19/2_2^-$	n.o.	—	0.00
	1733		$19/2_1^+$	0.24(8)	—	—
	1741		$19/2_1^-$	n.o.	—	0.00
	1816		$17/2_3^-$	n.o.	—	1.0
	2088		$17/2_2^-$	0.34(7)	—	0.00
	2639		$17/2_1^-$	0.42(20)	—	0.00
7295	*429*	$23/2_1^+$	$21/2_2^+$	n.o.	—	0.00
	575		$19/2_2^+$	n.o.	—	0.00
	1205		$21/2_1^+$	n.o.	—	0.00
	1743		$19/2_1^+$	1.0	—	1.0
7486	*620*	$25/2_1^+$	$21/2_2^+$	n.o.	—	0.00
	1396		$21/2_1^+$	1.0	—	1.0
7629	*152*	$23/2_1^-$	$21/2_2^-$	n.o.	—	0.00
	345		$21/2_1^-$	0.04(1)	—	0.02
	974		$19/2_2^-$	n.o.	—	0.98
	1538		$21/2_1^+$	0.96(12)	—	—
	2086		$19/2_1^-$	n.o.	—	0.00
8879	*149*	$25/2_1^-$	$23/2_2^-$	n.o.	—	0.00
	162		$21/2_3^-$	n.o.	—	0.00
	1250		$23/2_1^-$	n.o.	—	0.00
	1402		$21/2_2^-$	n.o.	—	0.00
	1595		$21/2_1^-$	1.0	—	1.0
9161	*194*	$27/2_1^-$	$25/2_3^-$	n.o.	—	0.00
	241		$25/2_2^-$	n.o.	—	0.00
	282		$25/2_1^-$	n.o.	—	0.00
	431		$23/2_2^-$	n.o.	—	0.00
	1532		$23/2_1^-$	0.61(14)	—	0.99
	1675		$25/2_1^+$	0.39(21)	—	—
10155	*96*	$31/2_1^-$	$29/2_1^-$	n.o.	—	0.00
	994		$27/2_1^-$	1.0	—	1.0

is the yrast 2270 keV $11/2^-$ level. Allowing all possible $\Delta I = 1$ and $\Delta I = 2$ transitions to states of lower energy results in four predicted transitions from the calculations. Of these only the 1273 keV and the 1005 keV transitions are experimentally observed and the branching ratios are determined as 0.73(3) and 0.27(3), respectively. Another example is the 756 keV $5/2^-$ yrare state, which experimentally decays via three well-known transitions (339, 632, 756 keV) and a tentative transition (667 keV). The four decays have observed branching ratios of 0.04(1), 0.05(1), 0.83(2), and 0.08(1), respectively. The calculation give the corresponding branching ratios as 0.05, 0.07, 0.88, and 0.00. The calculated results agree with the experimental ones for all but the tentative transition which is not predicted by the calculation.

One interesting detail noticed only in the analysis of the electromagnetic decay properties is the difficulty in reproducing the branching ratios for the yrast and yrare $3/2^-$ levels in the fp calculation. As can be seen in table 2 there are relatively large discrepancies between the experimental and the calculated results, especially for the $7/2_1^- \rightarrow 3/2_1^-$ transition. Experimentally, this is determined as 0.26(2) but the calculated branching ratio is as low as 0.01. The distinct difference is very surprising, especially when compared with the very good agreement between experimental and calculated branching ratios for all other yrast levels.

If two predicted levels with the same spin and parity are placed close in energy, shell model calculations have problems in correctly describing their electromagnetic decay properties. The problem can usually be solved by afterwards mixing the wave functions of the two states based on the matrix elements of the electromagnetic operators. However, in the current experiment *and* calculation the two $3/2^-$ states are separated by over 400 keV. Considering the MLD value of 228 keV obtained for this calculation —about 50% of the energy difference between the two levels of interest— the two states should be well separated, yet these difficulties persist.

The analysis of the branching ratios may also be used to predict weak transitions and provides a possibility to suggest spin assignments to new levels. One example, where this method can be applied, is the experimental level found at 3495 keV, which decays into the $9/2^-$ level with a γ-ray of 2229 keV. Based on the R_{154-96} value of 1.40(12) this transition is most likely to be of $\Delta I = 2$ character, which hints towards a 13/2 assignment to the 3495 keV level. Nevertheless, a mixed $\Delta I = 1$ transition cannot be ruled out. Theoretically, the $11/2_3^-$ and $13/2_3^-$ states are predicted at 3796 and 4519 keV. Using a $11/2_3^-$ assignment for the 3495 keV level, the main predicted decay branch (59%) corresponds to the observed 2229 keV γ-ray, while a $13/2_3^-$ at 3495 keV shall decay predominantly (47%) into the $13/2^-$ yrast state, which would be at variance with experiment. In conclusion, we tentatively associate the observed level at 3495 keV with the predicted $11/2_3^-$ state. In a similar way, the predicted $13/2_3^-$ and $15/2_3^-$ states are good candidates to explain the experimentally observed levels at 4309, and 4915 keV, respectively.

Comparing calculated and experimental energy levels, the $f_{5/2}pg_{9/2}$ calculation has already proven not to be equally reliable as the fp calculation. The study of the electromagnetic decay properties shows a similar trend and the values are also presented in table 2. This calculation provides predictions for positive- as well as negative-parity states, though it cannot predict any parity-changing $E1$ transitions. This is due to the fact that $\Delta I \geq 2$ for transitions between odd-ℓ ($2p_{3/2}$, $1f_{5/2}$, $2p_{1/2}$) and even-ℓ ($1g_{9/2}$) orbitals. Moreover, the $f_{5/2}pg_{9/2}$ calculation, due to the lack of the $1f_{7/2}$ orbital in the configuration space, underestimates the branching ratios of the

experimentally established parity-conserving $\Delta I = 1$ transitions. The difficulty originates from the K^2-dependence of the $B(M1)$ strength (see, *e.g.*, eq. 4-87 in ref. [19]). Excluding the $1f_{7/2}$ orbit will reduce the maximum of this value by almost a factor two. The effect is strikingly seen in the calculated branching ratios of the 1005 and 1273 keV transitions from the 2270 keV $11/2_1^-$ level. As mentioned above, the fp calculation reproduces them with very good precision, while the $f_{5/2}pg_{9/2}$ calculation reduces the $\Delta I = 1$ part to negligible 1%, it amounts to 27(3)% experimentally.

Finally, the experimentally obtained spin and parity assignments of low-lying states based on ref. [3] and the current analysis affect the tentative spin assignments of the superdeformed (SD) band presented in ref. [8]. The SD band will, according to previous analysis, decay into the 6090 and 7629 keV levels in the normally deformed level scheme, which now have fixed spin and parity assignments of $21/2^+$ and $23/2^-$, respectively. In the following, we have to assume that the 1432 keV transition at the bottom of the SD band (cf. ref. [8]) belongs to the band, *i.e.*, that it has $E2$ character. As a result, spin and parity $I^\pi = 23/2^-$ is assigned to the SD band head at 11367 keV, different from the tentative $I = 25/2$ assignment in ref. [8]. The modification of the spin assignment also leads to a change of signature, α, of the SD band in ^{61}Zn. Subsequently, the change of signature from $\alpha = +1/2$ to $\alpha = -1/2$ affects the discussion in ref. [8] in terms of proton and neutron occupancies of the $1g_{9/2}$ orbital for the band.

From the previous paper it is known that the SD occupancies in ^{61}Zn are built on the configuration of the SD band in ^{60}Zn. In ^{60}Zn two protons and two neutrons in the $1g_{9/2}$ orbital form the "doubly-magic" SD core in the mass region [20], and the additional neutron in ^{61}Zn can then occupy the positive-parity, $\alpha = +1/2$ Nilsson orbital [431]3/2, or either of the signatures in the [310]1/2 and the [303]7/2 orbitals. The latter orbital is unlikely since both of the two signature partners would be energetically close and, furthermore, they would be strongly coupled via cross-over $M1$ transitions connecting the levels between the bands (*e.g.*, structure 8 in ref. [1]). Neither of this is seen in the experimental data of ref. [8]. This leaves three possible Nilsson orbitals, two with $\alpha = +1/2$ and one with $\alpha = -1/2$. While the Skyrme-Hartree-Fock calculations in ref. [8] seem to energetically favour the two $\alpha = +1/2$ structures, Cranked Nilsson-Strutinsky (CNS) calculations [21,22] with standard parametrisation [21] predict the three remaining possibilities to be energetically equivalent within the spin regime the SD states are fed. More experimental work is clearly required to confirm that the lowest (11367 keV) level belongs to the SD band and/or that the 1432 keV γ-ray transition has $E2$ character and whether or not more bands exist in the second minimum of ^{61}Zn.

6 Summary

The current analysis of ^{61}Zn provides a firm, extended decay scheme involving almost 70 transitions with spins ranging up to $I^\pi = 31/2^-$. The experimentally obtained energy levels and branching ratios have been compared with predictions from large-scale shell model calculations involving the upper fp shell and either the $1f_{7/2}$ or the $1g_{9/2}$ orbital. The predictions prove to be in good agreement with the experimental results but neither is adequate to fully describe ^{61}Zn. With its well-known decay pattern and because it is placed in the middle of the upper fp shell ^{61}Zn, provides a good starting point for further developments of the shell model calculations.

The revised spin assignment of the SD band requires a modified analysis in terms of neutron and proton configurations and calls for further experimental investigations of the high-spin excitation scheme of the ^{61}Zn nucleus.

We would like to thank the staff and the accelerator crew at ORNL for the excellent support during the experiment and I. Ragnarsson for helpful discussions concerning the CNS calculations. Our gratitude also goes to E. Caurier for his help with and contribution to the shell model calculations. This research was supported in part by the Swedish Research Council and the U.S. DOE grant DE-AC05-000R22725.

References

1. C. Andreoiu *et al.*, Eur. Phys. J. A **14**, 317 (2002).
2. S.M. Vincent *et al.*, Phys. Rev. C **60**, 064308 (1999).
3. O. Izotova *et al.*, Phys. Rev. C **69**, 037303 (2004).
4. E. Caurier, G. Martínez-Pinedo, F. Nowacki, A. Poves, A.P. Zuker, Rev. Mod. Phys. **77**, 427 (2005).
5. L-L. Andersson *et al.*, Phys. Rev. C **71**, 011303(R) (2005).
6. M.R. Bhat, Nucl. Data Sheets **88**, 417 (1999).
7. R.B. Schubank, J.A. Cameron, V.P. Janzen, Phys. Rev. C **40**, 2310 (1989).
8. C.-H. Yu *et al.*, Phys. Rev. C **60**, 031305 (1999).
9. `www.phy.ornl.gov/hribf/equipment/clarion`.
10. C.J. Gross *et al.*, Nucl. Instrum. Methods Phys. Res. A **450**, 12 (2000).
11. T. Yamazaki, At. Data Nucl. Data Tables **3**, 1 (1967).
12. E. Gueorguieva, M. Kaci, C. Schück, A. Minkova, Ch. Vieu, J.J. Correia, J.S. Dionisio, Nucl. Instrum. Methods Phys. Res. A **474**, 132 (2001).
13. L.-L. Andersson, Licentiate thesis, Lund University, in preparation.
14. E. Caurier, Shell model code `ANTOINE`, IRES, Strasbourg (1989-2002).
15. E. Caurier, F. Nowacki, Acta Phys. Pol. **30**, 705 (1999).
16. M. Honma, T. Otsuka, B.A. Brown, T. Mizusaki, Phys. Rev. C **69**, 034335 (2004).
17. M. Honma, T. Otsuka, B.A. Brown, T. Mizusaki, Phys. Rev. C **65**, 061301 (2002).
18. E. Caurier, private communication.
19. A. Bohr, B. Mottelson, *Nuclear Structure*, Vol. **II**, ISBN 0-8053-1016-9 (v. 2) (1975).
20. C.E. Svensson *et al.*, Phys. Rev. Lett. **82**, 3400 (1999).
21. T. Bengtsson, I. Ragnarsson, Nucl. Phys. A **436**, 14 (1985).
22. A.V. Afanasjev, D.B. Fossan, G.J. Lane, I. Ragnarsson, Phys. Rep. **322**, 1 (1999).